UCRL-JC-126613
PREPRINT

A Late Miocene/Pliocene Origin of the Inverted Metamorphism of the Central Himalaya

T.M. Harrison
F.J. Ryerson
P. Le Fort
A. Yin
O.M. Lovera

This paper was prepared for submittal to the
Geological Society of America Abstracts with Progress Conference
Denver, CO
October 28-31, 1996

January 1997

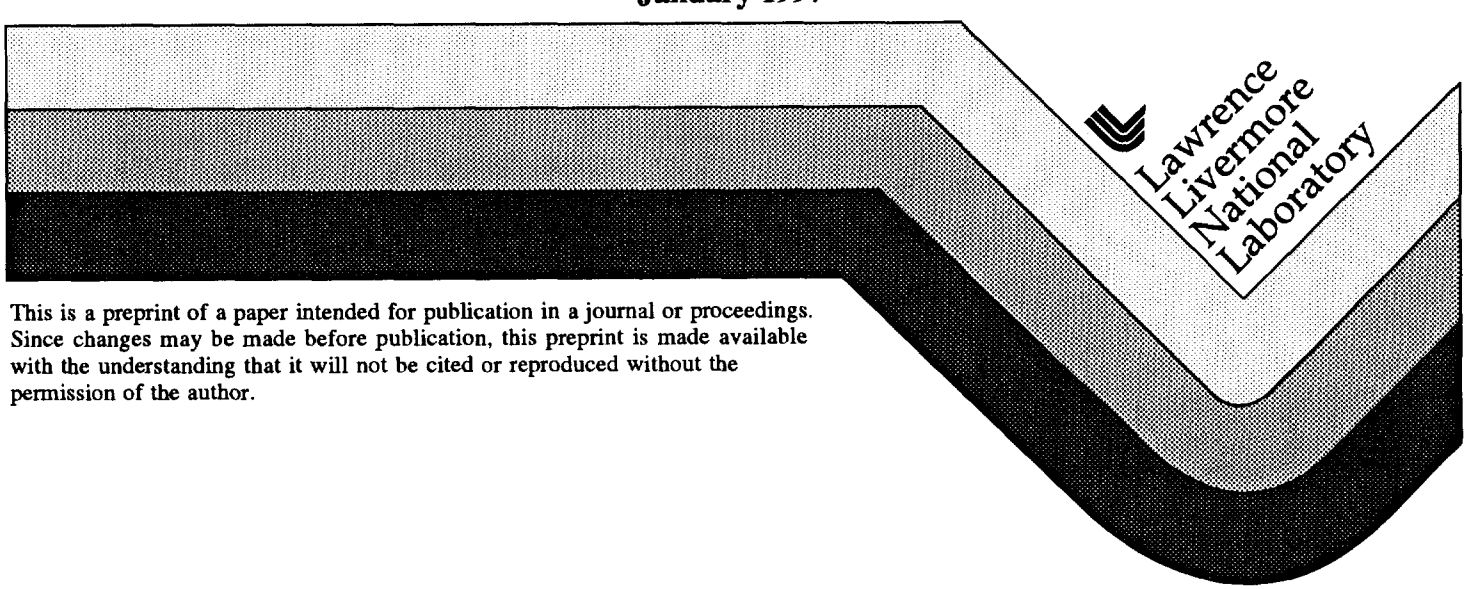

This is a preprint of a paper intended for publication in a journal or proceedings. Since changes may be made before publication, this preprint is made available with the understanding that it will not be cited or reproduced without the permission of the author.

DISCLAIMER

This document was prepared as an account of work sponsored by an agency of the United States Government. Neither the United States Government nor the University of California nor any of their employees, makes any warranty, express or implied, or assumes any legal liability or responsibility for the accuracy, completeness, or usefulness of any information, apparatus, product, or process disclosed, or represents that its use would not infringe privately owned rights. Reference herein to any specific commercial product, process, or service by trade name, trademark, manufacturer, or otherwise, does not necessarily constitute or imply its endorsement, recommendation, or favoring by the United States Government or the University of California. The views and opinions of authors expressed herein do not necessarily state or reflect those of the United States Government or the University of California, and shall not be used for advertising or product endorsement purposes.

A Late Miocene/Pliocene origin of the inverted metamorphism of the Central Himalaya

T. Mark Harrison, F.J. Ryerson*, P. Le Fort†, An Yin and Oscar M. Lovera

Department of Earth & Space Sciences and IGPP, University of California, Los Angeles, CA 90024, USA
*Lawrence Livermore National Laboratory, Livermore, CA 94550, USA
†Institut Dolomieu, C.N.R.S., Grenoble, 38301, France

The spatial association of intracontinental thrusting and inverted metamorphism, recognized in the Himalaya more than a century ago[1], has inspired continuing efforts to identify their causal relationship. Perhaps the best known sequence of inverted metamorphism is that found immediately beneath the Himalayan Main Central Thrust (MCT), generally thought to have been active during the Early Miocene. It has been widely assumed that the pattern of inverted metamorphism also developed at that time. Using a new approach, *in situ* Th-Pb dating of monazite included in garnet, we have discovered that the peak metamorphic recrystallization recorded in the footwall of the MCT fault occurred at ca. 5 Ma. The apparent inverted metamorphism resulted from activation of a broad shear zone beneath the MCT zone which juxtaposed two right-way-up metamorphic sequences. Recognition of this remarkably youthful phase of metamorphism resolves outstanding problems in Himalayan tectonics, such as why the MCT (and not the more recently initiated thrusts) marks the break in slope of the present day mountain range, and transcends others, such as the need for exceptional conditions to explain Himalayan anatexis.

Despite its role in absorbing a significant fraction of Indo-Asian convergence, fundamental issues regarding the evolution of the MCT, such as the timing of its initiation and cessation, remain poorly known. As all the major geologic elements of the Himalaya (i.e., leucogranites, South Tibet Detachment System (STDS), and inverted metamorphism; Fig. 1) have been related to the evolution of the MCT[2,3,4], establishing its slip history is key to understanding the nature of this unique orogenic belt. Although the question of a genetic link between Early Miocene anatexis in the MCT hanging wall and slip on the MCT and STDS is being debated[4-8], there has been no disagreement that Himalayan inverted metamorphism is temporally related to Early Miocene activity on the MCT.

The S-directed thrust faults of the Himalaya, principally the MCT and the Main Boundary Thrust, appear to sole in a common decollement at depth[9-12] (Fig. 1). In general, the MCT places high-grade gneisses of the Tibetan

Slab (= Greater Himalayan Crystallines) atop schists of the Midlands Formations (= Lesser Himalayan Formations), and the Main Boundary Thrust juxtaposes those schists against unmetamorphosed Neogene molasse (Fig. 1). Studies of the MCT hanging wall indicate that deformation and anatexis were occurring at 22±1 Ma, while cooling ages in the upper portion of the Tibetan Slab suggest that ductile deformation had ceased there by ~18 Ma[8,13-15]. The amount of slip along the MCT is inferred to be about 150-300 km, based on flexural modeling of gravity data and balanced cross-sections[16-19].

Juxtaposition of the Tibetan Slab atop the Midlands along much of the Himalaya is associated with a zone of inverted metamorphism that has long intrigued geologists (Fig. 2). Proposed causes of the apparent increase in metamorphic grade with higher structural position (i.e. shallower depth) include; the heating of the colder lower plate by emplacement of a hot nappe, either due to thermal relaxation alone or aided by strain heating[10,20-25], the folding of pre-existing isograds[26], imbricate thrusting[27], mantle delamination[46], and the ductile shearing of an existing zone of right-way-up metamorphism[28]. Within the central Himalaya, the Tibetan Slab increases in thickness from ~3 km in the Kali Gandaki section to >10 km in the Burhi Gandaki section (Fig. 1). This correlates with an eastward increase in thickness and peak grade of the inverted metamorphic section, reaching kyanite grade at Darondi Khola and corundum grade at Ankhu Khola (Fig. 1). The metamorphism within the Midlands (Fig. 2) typically increases in grade over a N-S distance of 10-20 km from chlorite through biotite, garnet, and kyanite, reaching sillimanite grade in the hanging wall[2]. The region approximately bounded by the garnet isograd and the MCT is usually characterized by a highly sheared, 4-8 km thick zone of distributed deformation (Fig. 2) commonly referred to as the 'MCT zone'[29-32]. Kinematic indicators within this broad zone document that the shear sense is uniformly top-to-the-south. Sheath folds, asymmetric boudinage, mylonitic gneisses with S-C fabrics, and S-verging isoclinal folds are abundant.

We examined the accessory mineralogy of pelites from the Midlands of central Nepal, which vary from chlorite grade in the structurally lowestmost samples to kyanite grade directly adjacent to the MCT (Fig. 2), with the goal of establishing the timing of inverted metamorphism. Monazite [$CePO_4$] is unstable in pelitic rocks during diagenesis and does not reappear until a temperature of ~500°C is reached[33-36]. During the period of instability, the constituents of monazite are carried either by allanite or light rare earth element (LREE) oxides[33-36]. Provided temperature does not greatly exceed 600°C[37], diffusive loss of radiogenic Pb (Pb*) produced by *in situ* decay of Th and U in monazite

is not significant. SEM studies of our rocks indicate that at chlorite and biotite grades, allanite is the principal host of LREE. Monazite overgrowths begin to appear on allanite hosts close to the garnet isograd and ~10-50 μm-sized neoformed monazites are present within the garnet grade rocks.

Four monazite grains identified in a thin section of sample AP332 (Fig. 2) were analyzed using the $^{208}Pb/^{232}Th$ ion microprobe method[8]. This technique is well-suited to determining *in situ* crystallization ages of Tertiary monazites as it permits textural relationships between monazite and mineral host to be retained, and the spatial selectivity permits inherited monazite cores to be identified and avoided. Th concentrations are typically very high in monazite (~3-8%) which, coupled with low levels of common Pb, results in relatively high levels of $^{208}Pb^*$ in young samples. The short time scale for secular equilibrium to be achieved among the intermediate daughters of ^{232}Th precludes monazite from containing excess $^{208}Pb^*$. The high $^{208}Pb^*$ abundances and high ionization efficiency of Pb from monazite under O_2^- bombardment[8] permit Th-Pb age determinations to be made in a ~10 μm spot on a *ca.* 5 Ma specimen in ~20 min. Ages are determined by direct reference to a standard, in this case 554 monazite which yields a $^{208}Pb/^{232}Th$ isotope dilution age of 45±2 Ma[47]. The standard calibration has a typical reproducibility of ±2%[8]. Performing the ion microprobe measurements in polished section rather than as separated grains in an epoxy mount has presented no technical difficulties. The regions within the polished thin section containing monazite were isolated by sawing and then mounted with several grains of 554 monazite in a 1" diameter epoxy mount and Au coated for analysis (see ref. 8 for additional details of analytical methods).

Based on previous geochronological studies of the Tibetan Slab[8,15], our expectation was that crystallization ages might range from ~20 to >30 Ma. Surprisingly, four different monazite grains yield $^{208}Pb/^{232}Th$ ages between 4.5 and 8.0 Ma (Table 1). Of potentially greatest significance is a monazite grain included within a mm-sized garnet in AP332 (Fig. 3). Garnet-biotite-plagioclase-muscovite-quartz thermobarometry (see ref. 38) for this sample yields a P-T of 6-8 kbar and 550±30°C, typical of conditions found within the MCT zone in this region[32]. Since chlorite would have become unstable had the pressure exceeded ~8 kbar[38], the presence of abundant primary chlorite in AP332 suggests that the pressure estimate reflects the peak value. The two Th-Pb measurements on this grain yield an average age of 5.6±0.1 Ma. Since the garnet and monazite isograds are essentially coincident in temperature (i.e., ~525°C), we conclude that these data are *prima facie* evidence that garnet growth in the presently exposed rocks was occurring at a depth of ~25 km at ~5-6 Ma. Preliminary measurements of monazite in garnet from sample DH-73-

96, Darondi Khola (Fig. 1), yield ages between 9-11 Ma which, though somewhat older, are consistent with the pattern of inverted metamorphism in the central Himalaya being established during the Late Miocene.

Several other lines of evidence also suggest that the MCT was active during the Pliocene. $^{40}Ar/^{39}Ar$ ages[13] from a N-S section through the Darondi and Burhi Gandaki valley's drop from ~16 Ma in the upper MCT hanging wall to ~4 Ma within and adjacent to the MCT zone before climbing to pre-Tertiary ages (Fig. 4d). A U-Ti oxide precipitated in an albitic alteration zone within the Tibetan Slab yielded U-Pb ages of 4.8-5.2 Ma[13]. Although these young ages were previously ascribed, respectively, to isotopic resetting and crystallization due to hot fluids channeled along the MCT at 5 Ma[13], the ~7 kbar pressure recorded by AP332 rules out this interpretation. This is because both the upper portion of the Tibetan Slab and the lower grade portion of the Midlands are known from thermochronometry[13,14] to have been relatively cold, and therefore relatively close (<15 km) to the Earth's surface, at 5 Ma when AP332 was at a depth of ~25 km. Although wedge extrusion (e.g., ref. 4) of the MCT zone during the Pliocene can explain the pattern of mineral ages (Fig. 4d), this mechanism would require the MCT to have been reactivated as a normal fault and field evidence for a top-to-the-south relationship across the MCT zone is overwhelming[2,32]. The hypothesis we favor is that, following termination of a phase of slip during the Early Miocene, the MCT was reactivated during the Late Miocene. Slip was initially restricted to the MCT fault and resulted in the burial metamorphism of the upper Midlands (as recorded by sample AP332). Uplift induced advection of heat within the hanging wall may have driven fluid circulation and produced the localized greenschist alteration[13]. In a second phase of deformation, strain was accommodated across the broad MCT shear zone resulting in juxtaposition of two right-way-up metamorphic sequences (see ref. 28).

We have consolidated our observations in the framework of a numerical model in order to constrain a variety of possible Late Miocene/Pliocene deformation histories that are consistent with our thermobarochronologic result. We assume that the MCT was the footwall ramp in a fault-bend thrust geometry[39] and use a finite-difference solution to the diffusion-advection equation to test models involving both hanging wall deformation alone and combined hanging wall and footwall deformation. An example of the latter model which closely matches our isotopic constraints is shown in Fig. 4. In this model, the MCT fault is activated at 8 Ma (following 12 m.y. of inactivity) with a total displacement rate of 22 mm/yr (Fig. 4a). At 6 Ma, activity shifts from the northern to the southern boundary of the MCT zone (Fig. 4b). Although the MCT zone is without question a broad shear zone (yellow in

Fig. 4a,b), for simplicity we have modeled it as a single fault at the base of the shear zone. In either case, the net effect is that garnet grade Midlands rocks are accreted to the hanging wall, which continues to be transported up the ramp. Slip terminates at 4 Ma. Together with the kinetic parameters for Ar diffusion in biotite[40], the calculated thermal histories corresponding to mineral dating localities predict a biotite age distribution (solid curve) that closely matches the empirical results[13] (Fig. 4d). The model also predicts that the presently exposed upper Midlands would have reached the garnet isograd at ~6 Ma at a *P-T* of 7 kbar and 550°C, in excellent agreement with the monazite-in-garnet result for AP332 (square in Fig. 4c).

Thermobarometry[41] of rocks collected in a roughly horizontal N-S traverse through the Tibetan Slab indicate that pressures as high as ~7 kbar were achieved adjacent to the MCT, whereas peak pressures at the top of the section were only ~3-4 kbar. When pressure is plotted against inferred structural height above the MCT, these results yield a 'normal' lithostatic gradient of 0.27 kbar/km[41] implying that these rocks were once sub-vertical and subsequently rotated ~30°. Our numerical model predicts that hanging wall rocks from the range of depths corresponding to these pressures would today be exposed at the surface together as a result of the rotation associated with their sequential transport up the ramp (see Fig. 4b). Although the results of our thermal modeling are not unique, particularly with respect to the timing of activation of the MCT zone, they demonstrate both the physical plausibility of our hypothesis and that a wide variety of observations can be reconciled within its framework.

If Late Miocene activation of the MCT zone and the subsequent development of inverted metamorphism were a widespread occurrence across the Himalaya, two long-standing geodynamic and geomorphological puzzles would be easily resolved. Although the surface expression of the presently active Main Frontal Thrust and recently active Main Boundary Thrust are exposed at elevations of <1 km, it is the MCT zone that marks the most dramatic topographic break in slope within the Himalaya[42,43]. If the MCT zone had been inactive for the past ~20 m.y., why would this feature persist? Although a shallow (~15°) ramp on the decollement[44] at ~20 km depth may be a contributory factor in elevating the MCT zone, it would not produce a sharp break in slope over such a short distance unless the overlying rocks were unusually flexurally weak. More likely, this feature simply reflects the fact that significant displacement along the MCT zone was occurring as recently as 4 Ma. The one common element among the numerous attempts to account for the thermal energy required by Tibetan Slab anatexis is the requirement for some extraordinary process to have aided melting. A variety of special mechanisms have been proposed, including

high (100 MPa) shear stress along the MCT[23], mantle delamination[46], very long (>25 m.y.) or short (≤1 m.y.) thermal incubation periods[24,25], high concentrations (many 100's of ppm) of B, F, and Li[45], or rapid (>5 mm/yr) decompression[6]. Although the juxtaposition of rocks undergoing partial melting with the relatively cold rocks of the adjacent MCT zone undergoing endothermic reactions[10] appears enigmatic, our hypothesis provides a simple explanation. The (presumably higher grade) footwall rocks that were juxtaposed against the thrust flat of the MCT during anatexis have since been displaced northward and replaced by a tectonically telescoped section of lower grade rocks. As a consequence, any attempt to explain the present juxtaposition of Tibetan Slab and Midlands Formations without recognizing the diachroneity of deformation is ordained to require extraordinary circumstances.

1. Oldham, R.D., *Rec. Geol. Surv. India* **16**, 193-198 (1883).
2. Colchen, M., Le Fort, P., & Pêcher, A. *Annapurna-Manaslu-Ganesh Himal notice de la carte geologiquie au 1/200.00e* Bilingual edition: French-English. Paris: Centre Nationalde la Recherche Scientifique (1986).
3. LeFort, P., Cuney, M., Deniel, C., France-Lanord, C., Sheppard, S.M.F., Upreti, B.N., & Vidal, P., *Tectonophysics* **134**, 39-57 (1987).
4. Burchfiel, B.C., Chen, Z., Hodges, K.V., Liu Y., Royden, L.H., Deng, C., & Xu, J. *Geol. Soc. Am. Spec. Pap.* **269**, 41 p. (1992).
5. Yin, A. *Jour. Geophys. Res.* **98**, 14,245-14,256 (1993).
6. Harris, N. & Massey, J. *Tectonics* **13**, 1537-1546 (1994).
7. Le Fort, P. in *The Tectonics of Asia* (eds. A. Yin & T.M. Harrison), Cambridge University Press, 95-109 (1996).
8. Harrison, T.M., McKeegan, K.D., & LeFort, P. *Earth Planet. Sci. Lett.* **133**, 271-282 (1995).
9. Gansser, A. *The Geology of the Himalayas*, Wiley Interscience, New York, 289 p. (1964).
10. Le Fort, P. *Am. J. Sci.* **275A**, 1-44 (1975).
11. Burbank, D.W., Beck, R.A. & Mulder, T. in *The Tectonics of Asia* (eds. A. Yin & T.M. Harrison), Cambridge University Press, 149-188 (1996).
12. Zhao, W. et al., *Nature* **366**, 557-559 (1994).
13. Copeland, P. , Harrison, T.M., Hodges, K.V., Maréujol, P., LeFort, P., & Pêcher, A. *Jour. Geophys. Res.* **96**, 8475-8500 (1991).
14. Hubbard, M.S. & Harrison, T.M. *Tectonics* **8**, 865-88 (1989).
15. Parrish, R.R. & Hodges, K.V. *Geol. Soc. Am. Abs. w. Progs.* **25**, A174 (1993).
16. Lyon-Caen, H. & Molnar, P. *Tectonics* **4**, 513-538 (1985).
17. Schelling, D. *Tectonics*, **11**, 925-943 (1992).
18. Schelling, D. & Arita, K. *Tectonics* **10**, 851-862 (1991).
19. Srivastava, P. & Mitra, G. *Tectonics* **13**, 89-109 (1994).
20. Arita, K. *Tectonophysics* **95**, 43-60 (1983).
21. Graham, C.M. & England, P.C. *Earth Planet. Sci. Lett.* **31**, 142-152 (1976).
22. England, P. & Thompson, A.B. *J. Petrol.* **25**, 894-928 (1984).
23. Molnar, P. & England, P. *J. Geophys. Res.* **95**, 4833-4856 (1990).
24. England, P., Le Fort, P., Molnar, P., & Pêcher, A. *Jour. Geophys. Res.* **97**, 2107-2128 (1992).
25. England, P. & Molnar, P. *Tectonics* **12**, 145-157 (1993).
26. Searle, M.P. & Rex, D.C. *J. Metamorph. Geol.* **7**, 127-134 (1989).
27. Brunel, M., & Kienast, J.R. *Can. J. Earth Sci.* **23**, 1117-1137 (1986).
28. Hubbard, M.S. *J. Geol.* **104**, 1996.
29. Hubbard, M.S. Ph.D. dissertation, Mass. Inst. Tech., 1988.
30. Bouchez, J.L. & Pêcher, A. *Tectonophysics* **78**, 23-50 (1981).
31. MacFarlane, A.M. *Jour. Metamorph. Geol.* **13**, 595-612 (1995).
32. Pêcher, A. *J. Metamorph. Petrol.* **7**, 31-41 (1989).
33. Overstreet W.C. *U.S. Geol. Surv. Prof. Paper* **530**, 327 p. (1967).
34. Smith, H.A. & Barreiro, B. *Contrib. Mineral. Petrol.* **105**, 602-615 (1990).

35. Harrison, T.M., Kingsbury, J.A. & Miller, C.D. *2nd Goldschmidt Conf. Abs*, 52 (1990).

36. Kingsbury, J.A., Miller, C.F., Wooden, J.L. & Harrison, T.M. *Chem. Geol.* **110**, 147-168 (1993).

37. Smith, H.A. & Giletti, B. *EOS* **75**, 692 (1994).

38. Spear, F.S. *Metamorphic Phase Equilibria & Pressure-Temperature-Time Paths*, Washington, D.C.: Mineralogical Society of America Monograph, 799 p. (1993).

39. Suppe, J. *Am. J. Sci.* **283**, 684-721 (1983).

40. Grove, M. & Harrison, T.M. *Am. Min.* **81**, 940-951 (1996).

41. Hodges, K.V., Le Fort, P. & Pêcher, A. *Geology* **16**, 707-710 (1988).

42. Nakata, T. in *Tectonics of the Western Himalaya* (eds. L.L. Malinconico & R.J. Lillie), Spec. Pap. Geol. Soc. Am. 232, 243-264 (1989).

43. Masek, J.G., Isacks, B.L., Gubbels, T.L. & Fielding, E.J. *Jour. Geophys. Res.* **99**, 13,941-13,956 (1994).

44. Yeats, R.S. *Abstracts of the 11th Himalayan-Karakorum-Tibet Workshop*, Flagstaff, AZ, April 29-May 1, 1996, 171-172 (1996).

45. Guillot, S. & Le Fort, P. *Lithos* **35**, 221-234 (1995).

46. Bird, P. J. Geophys. Res. 83, 4975-4987 (1978).

47. M. Tatsumoto, personal communication, 1995.

Acknowledgments

We thank Kevin McKeegan and Chris Coath for their assistance with the ion microprobe measurements and Dan Farber for the SEM characterization of AP332. This research was supported by grants from the NSF. We particularly wish to thank the directors and staff of the W.M. Keck Foundation for their generous support.

Support for this research was provided by The Geophysics and Planetary Physics-Lawrence Livermore National Laboratory and worked performed under the auspices of the U.S. Department of Energy by Lawrence Livermore National Laboratory under Contract W-7405-Eng-48.

Table 1. Th-Pb ion microprobe monazite ages

grain	spot	$^{208}Pb/^{232}Th$ age (%)[1]	$^{208}Pb^*$ (Ma)
1	1	24	5.7±0.7
	2	84	8.0±0.4
2	1	81	*5.5±0.2*
	2	87	*5.7±0.1*
5	1	34	6.0±0.9
6	1	28	4.6±0.8
	2	77	5.0±0.3
	3	80	5.5±0.2

[1]Calculated assuming common $^{208}Pb/^{204}Pb = 39.5$

Fig. 1 Geological sketch map of the Himalaya and Southern Tibet (after ref. 3) showing the relationship between the Tibetan Slab and Midlands Formations including reference isograds of the inverted metamorphic section. The Tibetan Slab is juxtaposed against the Tethyan metasediments by the STDS. The section marked A-A' is shown in Fig. 2. KG = Kali Gandaki, BG = Burhi Gandaki, D = Darondi Khola, AK = Ankhu Khola.

Fig. 2 Generalized cross section through the central Himalaya (after ref. 2) illustrating the pattern of inverted metamorphism beneath the Main Central Thrust (MCT). MBT = Main Boundary Thrust, STDS = Southern Tibetan Detachment System. The projected location of sample AP332 is shown.

Fig. 3 Reflected light photomicrograph of sample AP332 showing garnet (gt) in a biotite (bi) and quartz (qt) matrix. Thermobarometry yields a P-T of 7±1 kbars and 530±30°C. Two Th-Pb analyses of the monazite inclusion yield an average age of 5.6±0.1 Ma indicating garnet formation occurred at the time at a depth of ~25 km. The discolored region near the monazite is where the Au coating has been removed by sputtering.

Fig. 4 Thermal modeling was undertaken assuming a fault-bend fold geometry, with top and bottom boundaries maintained at constant temperatures of 25°C and 1025°C, respectively, (resulting in an initial thermal gradient of 25°C/km) and reflecting side boundaries. Denudation equals surface uplift, although topography was simulated in some runs. In this model, both the hanging wall and footwall move at 11 mm/yr in opposite directions. (a) Slip along the MCT begins at 8 Ma. Hanging wall rocks are first transported along the flat and then up the ramp. NL25, the sample closest to the MCT and thus at the highest peak pressure (~7 kbar), is the first to reach the MCT (see refs. 13, 41). It is followed sequentially up the ramp by U129 (~6 kbar) and U752 (~4 kbar) (see refs. 13, 41). Between 8 and 6 Ma, sample AP332 experiences burial heating due to overthrusting by the Tibetan Slab. (b) At 6 Ma, the MCT zone (modeled as a single fault at the base of the shear zone) is activated accreting the garnet grade Midlands rocks, formed by thrusting beneath the Tibetan Slab, onto the hanging wall which continues to be transported up the ramp. Slip terminates at 4 Ma. (c) Temperature histories predicted by the thermal model for Tibetan Slab samples NL25, U129, U752, MCT zone sample AP332, and sample AP524 from beneath the MCT zone. The model predicts that the exposed MCT zone would have reached the garnet isograd at ~6 Ma at a *P-T* of 7 kbar and 550°C, in agreement with AP332 result (box; Table 1). (d) Biotite ages from a N-S traverse across the MCT zone and into the Tibetan

Slab (ref. 13). The thermal histories calculated by numerical model predict biotite ages (black curve) that closely match the observed distribution.

Technical Information Department • **Lawrence Livermore National Laboratory**
University of California • Livermore, California 94551